PREPRINT: Blocken B, Carmeliet J, Stathopoulos T. 2007. CFD evaluation of the wind speed conditions in passages between buildings – effect of wall-function roughness modifications on the atmospheric boundary layer flow. Journal of Wind Engineering and Industrial Aerodynamics 95(9-11): 941-962. © Elsevier 2007.

CFD evaluation of wind speed conditions in passages between parallel buildings – effect of wall-function roughness modifications for the atmospheric boundary layer flow

Bert Blocken* [(a)], Jan Carmeliet [(a,b)], Ted Stathopoulos [(c)]

(a) Unit Building Physics and Systems, Technische Universiteit Eindhoven, P.O. box 513, 5600 MB Eindhoven, the Netherlands
(b) Laboratory of Building Physics, Katholieke Universiteit Leuven, Kasteelpark Arenberg 40, 3001 Leuven, Belgium
(c) Department of Building, Civil and Environmental Engineering, Centre for Building Studies, Concordia University, 1455 de Maisonneuve Blvd West, H3G 1M8, Montreal, Quebec, Canada

Abstract

A numerical study of the wind speed conditions in passages between parallel buildings has been conducted for a wide range of passage widths with the commercial CFD code Fluent 6.1.22. CFD validation has been performed by comparison of the numerical results with the corresponding wind tunnel measurements. The study shows that accurate CFD simulation of a horizontally homogeneous atmospheric boundary layer (ABL) flow and of the subsequent building-related flow might be seriously compromised by the use of the wall-function roughness modifications present in many commercial CFD codes. In addition, the simulation results indicate that, at least for the cases studied here, the increase of wind speed in passages is only pronounced at the pedestrian level and that the flow rate through the passage is at most only 8% higher than the free-field flow rate, indicating that the so-called Venturi-effect is rather weak.

Keywords: Wind flow; Building; Numerical simulation; Computational Fluid Dynamics; Validation; Wall function; Roughness modification; Atmospheric boundary layer; Horizontal homogeneity; Flow stability; Pedestrian wind environment; Venturi effect

1. Introduction

Passages between buildings are ubiquitous. Experience, wind tunnel measurements and Computational Fluid Dynamics (CFD) simulations have led to the common knowledge that wind speed values in passages can be significantly increased. Different types of passages between buildings can be distinguished. Examples are passages between parallel buildings that are placed side-by-side, passages between parallel shifted buildings and passages between non-parallel buildings. The study in this paper is confined to the first type.

Many studies on wind conditions in passages between parallel side-by-side buildings have been conducted in the past, by wind tunnel modelling and, more recently, by numerical simulation. Most of these studies focused on pedestrian-level winds. Two main categories can be distinguished: (1) Fundamental studies, which are typically conducted for simple, generic building configurations to obtain insight in the flow behaviour, to study the influence of different building dimensions and passage widths, to provide input for knowledge-based expert systems (KBES) and/or for model validation. (2) Applied studies, which provide knowledge of the wind environmental conditions in specific and often much more complex case studies. Fundamental studies have been conducted by e.g. Ishizaki and Sung (1971) and by Wiren (1975), who carried out wind tunnel measurements along the passage centre line between various two-building configurations. Both studies focused on the mean wind speed in passages between block-type buildings of equal height. In the study by Stathopoulos and Storms

* Corresponding author: Bert Blocken, Unit Building Physics and Systems, T.U.Eindhoven, P.O.Box 513, 5600 MB Eindhoven, the Netherlands. Tel.: +31 (0)40 247 2138, Fax +31 (0)40 243 8595
E-mail address: b.j.e.blocken@tue.nl

(1986), the influence of different building heights and different wind directions on the wind conditions in the passages was investigated. Also, as opposed to earlier studies, information on turbulence intensity in the passages was provided. Later, additional measurements were made to support empirical formulae for KBES (Stathopoulos et al. 1992). The previous studies focused on wind speed conditions along the passage centre line. Contours of mean wind speed and turbulence measurements at pedestrian level in passages between two high-rise buildings of equal height were provided by To and Lam (1995), for parallel and for perpendicular wind direction. Wind tunnel studies of flow within structured multiple-building arrangements are reported by – among others – Stathopoulos and Wu (1995), Chang and Meroney (2001) and in the CEDVAL database by the Environmental Wind Tunnel Laboratory (EWTL) of the Meteorological Institute at Hamburg University (www.mi.uni-hamburg.de/cedval) (Leitl and Schatzmann 1999; Leitl 2000). Numerical studies for two-building models were conducted by Bottema (1993) and by Baskaran and Kashef (1996). Other valuable studies – but not of interest for the present paper – are those focusing on wind blowing perpendicular to the passage. In addition, a large number of applied studies are reported in the literature.

All the above-mentioned studies indicate that significantly increased wind speed can occur in the passages at pedestrian level. Amplification factors up to 1.4 have been reported at the passage centre line. The amplification factor is defined as the ratio of the mean wind speed at a certain location to the mean wind speed at the same location without the buildings present. As such it is a direct indication of the effect of the buildings on the wind speed. In the past, studies on wind speed conditions in passages were mainly focused on pedestrian-level winds (1.75 to 2 m height above ground) and were generally conducted for a limited range of passage widths. On several occasions, the increased wind speed values in these passages have been attributed to the Venturi-effect, meaning that the wind speed in the passage is increased due to the decrease of the flow section. However, a detailed analysis of the wind speed conditions above pedestrian-level in passages and of the Venturi-effect in these passages has not yet been performed. In addition, the adequacy and accuracy of CFD for this type of studies is an issue of debate, and more validation studies are needed.

CFD simulations of flow over rough surfaces generally require the use of wall functions to include empirical information about the roughness effects in the simulation. For wind flow in the Atmospheric Boundary Layer (ABL), the results of CFD simulations are highly dependent on the type of roughness modification applied to the wall functions. Many commercial CFD codes provide only one option to the user: wall functions modified for roughness based on empirical formulae for sand-grain roughness, e.g. those proposed by Cebeci and Bradshaw (1977) based on Nikuradse's data for roughened pipes and channels. Questions about the adequacy of this approach for ABL flow modelling in Computational Wind Engineering have been raised before (e.g. Westbury and Miles 2003; Franke et al. 2004; Blocken and Carmeliet 2005; Franke and Frank 2005) but its effect on the simulation results for wind flow around buildings has – to the knowledge of the authors – not yet been investigated.

This paper examines the validity of computational results in passages between buildings by comparing them with the relevant wind tunnel data. In Section 2, the effect of the roughness modification in the wall functions on the simulation of ABL flow is outlined. In Section 3, its effects for the accuracy of CFD simulations in passages between buildings are illustrated and an attempt is made to correct the results. Finally, in Section 4, the corrected results are used to analyse the wind speed conditions between two parallel buildings for a wide range of passage widths and to investigate the extent to which the Venturi-effect contributes to the increased wind speed in the passages.

2. Numerical simulation of atmospheric boundary layer flow

2.1. Requirements for atmospheric boundary layer flow simulation in Wind Engineering

In CFD simulations of the ABL where an accurate description of the flow near the ground surface is required – which is the case in almost all Wind Engineering studies – and where the wall roughness is expressed by an physical roughness height K_S in the wall functions, four requirements should be simultaneously satisfied:

(1) A sufficiently high mesh resolution in the vertical direction close to the ground surface;
(2) A horizontally homogeneous approach flow;
(3) A distance y_P from the centre point P of the wall-adjacent cell to the wall (ground surface) that is larger than the physical (or geometrical) roughness height K_S ($y_P > K_S$); and
(4) The relationship between the physical roughness height K_S and the aerodynamic roughness length y_0 denoting that y_0 is only a small fraction of K_S (Durbin and Petterson Reif 2001):

$$K_S \approx 30 y_0 \quad (1)$$

The first requirement is important for all Computational Wind Engineering studies, especially for those focusing on pedestrian wind environment. Franke et al. (2004) state that at least 2 or 3 control volume layers should be provided below pedestrian height (1.75 or 2 m full scale). The second requirement, i.e. horizontal homogeneity of the vertical mean wind speed and turbulence profiles, refers to the absence of streamwise gradients in the flow (Richards and Hoxey 1993). This implies that the flow profiles imposed at the inlet and travelling through the computational domain should remain free of all streamwise gradients, at least up to the location of the upstream disturbance by the building. The third requirement implies that it is not physically meaningful to have grid cells with centre points within the physical roughness height. This requirement is also explicitly mentioned by several commercial CFD codes including Fluent 6.1. (Fluent Inc. 2003) and Ansys CFX 10.0. (Ansys 2005). Both codes warn the user to abide by the requirement $y_P > K_S$. In addition, Ansys (2005) mentions that violation of this requirement can lead to inaccuracies and to solver failure; however it does not elaborate further on this issue. Finally, the fourth requirement has to be satisfied for a fully rough surface and it inherently imposes the need to incorporate empirical information about the ground roughness (roughness of the bottom of the computational domain) in the simulation. This generally requires the use of wall functions, at least for the bottom of the domain. Generally, this is done by applying a roughness modification to the wall functions. Many commercial CFD codes, including Fluent 6.1.22 (used in this study) and Ansys CFX 10.0, provide a similar type of roughness modification.

2.2. Roughness modification of the wall functions

The roughness modification outlined in this subsection considers the standard wall functions by Launder and Spalding (1974) used in combination with the standard k-ε turbulence model. Note however that the validity of the findings is not limited to this type of wall functions and this turbulence model. The modified law-of-the-wall is:

$$\frac{U_p u^*}{u_\tau^2} = \frac{1}{\kappa} \ln\left(E \frac{u^* y_p}{\nu} \right) - \Delta B \quad (2)$$

where U_P is the tangential wind speed in the centre point P of the wall-adjacent cell, E is the empirical constant for a smooth wall (≈ 9.793), ν is the kinematic viscosity of the fluid, ΔB is a roughness function and u* and u_τ are the wall-function friction velocities defined as:

$$u^* = C_\mu^{\frac{1}{4}} k_p^{\frac{1}{2}} \quad (3)$$

$$u_\tau = \sqrt{\frac{\tau_w}{\rho}} \quad (4)$$

In Eq. (3) and (4), C_μ is a constant (often 0.09), k_P is the turbulent kinetic energy in point P, τ_w is the wall shear stress and ρ is the density of the fluid. It is noted that adding the roughness function ΔB in Eq. (2) corresponds to dividing the constant E in this equation by the exponential roughness function A:

$$A = \exp(\kappa \Delta B) \quad (5)$$

Experimental evidence for this type of roughness modification has been obtained from experiments in roughened pipes and channels. These have indicated that the mean velocity distribution near rough walls, when plotted in a semi-logarithmic scale, has the same slope (1/κ) but a different intercept. The roughness function ΔB is added to take into account the shift of the intercept due to roughness. It depends on the type (uniform sand, rivets, ribs, etc.) and size of the roughness. There is no universal roughness function that is valid for all types of roughness. Commercial CFD codes often adopt the correlation of ΔB with the non-dimensional roughness height K_S^+

$$K_S^+ = \frac{K_S u^*}{\nu} \tag{6}$$

which holds for a sand-grain roughness and for similar types of equivalent uniform roughness elements. The roughness function ΔB is not a single function of K_S^+ but it takes different forms depending on the K_S^+ value. Three regimes are distinguished: hydrodynamically smooth, transitional and fully rough. The formulae used to compute the roughness function ΔB can be those by Cebeci and Bradshaw (1977), Ligrani and Moffat (1986) or others. Fluent 6.1.22 uses the former for the following three types of flow regime:

Hydrodynamically smooth regime ($K_S^+ < 2.25$):

$$\Delta B = 0 \tag{7}$$

Transitional regime ($2.25 \le K_S^+ < 90$):

$$\Delta B = \frac{1}{\kappa} \ln\left[\frac{K_S^+ - 2.25}{87.75} + C_{Ks} K_S^+\right] . \sin\left[0.4258\left(\ln K_S^+ - 0.811\right)\right] \tag{8}$$

Fully rough regime ($K_S^+ \ge 90$):

$$\Delta B = \frac{1}{\kappa} \ln\left(1 + C_{Ks} K_S^+\right) \tag{9}$$

where C_{Ks}, the roughness constant, is an attempt to take into account the type of roughness. However due to the lack of specific guidelines, this is generally set at its default value for roughened pipes and channels: 0.5. The user inputs are the values K_S and C_{Ks}, with the restriction that C_{KS} should lie in the interval [0,1]. Based on these values, the value of the roughness function ΔB is computed and the modified law-of-the-wall (Eq. 2) is then used to evaluate the shear stress and the wall function for the turbulent dissipation rate

$$\varepsilon_P = \frac{C_\mu^{\frac{3}{4}} k_P^{\frac{3}{2}}}{\kappa\, y_P} \tag{10}$$

and to provide the input for solving the k-equation in the wall-adjacent cells. Although many commercial CFD codes usually provide several types of wall functions, generally only this or a very similar type of roughness modification is available. Note that Ansys CFX 10.0 only provides the smooth and fully rough regime with a fixed $C_{KS} = 0.3$, while Fluent 6.1.22 includes the transitional regime and the option to modify C_{KS}.

The actual relationship between K_S and y_0 for the fully rough regime can be derived by first-order continuity fitting of the ABL log law and the wall-function log law including the appropriate roughness function (Eq. 2) at height $y = y_P$. This relationship depends on the type of roughness function. Based on the data by Ligrani and Moffat (1986), it is as indicated in Eq. (1), while from the data by Cebeci and Bradshaw (1977), it is given by:

$$K_S \approx \frac{E}{C_{KS}} y_0 = \frac{9.793}{C_{KS}} y_0 \tag{11}$$

which yields $K_S \approx 20 y_0$ for the default value $C_{KS} = 0.5$ and $K_S \approx 30 y_0$ for $C_{KS} = 0.327$.

2.3. Conflict in the requirements for ABL flow simulation

With the roughness modification outlined above, satisfying all four requirements in CFD simulations of near-ground ABL flows is generally impossible. The main reason is that Eq. (1) or (11) in combination with the third requirement mentioned in subsection 2.1, implies that very large (high) control volumes should be used, which is in conflict with the first requirement. As an example, for a grass-covered plain with a low aerodynamic roughness length $y_0 = 0.03$ m (Wieringa 1992), K_S is about 0.6-0.9 m and y_P should be at least equal to this value, yielding cells of minimum 1.2-1.8 m height (all full-scale values). For larger values of y_0, much larger (higher) cells are needed. Clearly, this requirement conflicts with the need for a high grid resolution near the

bottom of the computational domain and no accurate solutions for near-ground flow can be obtained with cell sizes so large. This issue was also mentioned by Franke et al. (2004). In fact, a similar or the same value for K_S as for y_0 has been used on many occasions of CFD simulations, e.g. Richards and Younis (1990) discussing the work of Mathews (1987). The change in roughness between the inlet profile (with $K_{S,1} \approx 20y_0$ to $30y_0$) and the actual smaller ground roughness in the computational domain ($K_{S,2} = y_0$) introduces an Internal Boundary Layer (IBL) in which the wind speed and turbulence profiles rapidly adapt to the new and smaller roughness, yielding amongst others a considerable acceleration of the flow near the surface (horizontal inhomogeneity of the wind speed profile). This is schematically illustrated in Figure 1 and it implies that the flow profiles imposed at the inlet and the incident flow profiles (i.e. the profiles at the position in the domain where the buildings would be located) can be considerably different in CFD simulations. The difference depends on the inlet profiles of mean wind speed and turbulent quantities, the turbulence model used, the grid resolution (y_P), the type of wall function roughness modification, the values of K_S and C_{KS} and the upstream length of the computational domain. This problem and its effects on the accuracy of CFD simulations of building-related flow will be illustrated in the next section.

3. Numerical simulation and validation of wind speed conditions in passages

3.1. Wind tunnel measurements for CFD validation

The wind tunnel measurements by Stathopoulos and Storms (1986) are used for model validation. The measurements were conducted at a scale of 1/400 in the boundary layer wind tunnel of the Centre for Building Studies (CBS) (Stathopoulos 1984). These measurements were selected because the authors clearly reported the "incident" vertical wind speed and turbulence intensity profiles and not the "approach flow" profiles. In this paper, "incident" profiles in the wind tunnel are defined in the same way as for the CFD simulations: the profiles measured in the empty wind tunnel at the location where the buildings will be positioned. The so-called "approach" profiles are those measured at a certain distance upstream of the turntable and the model, outside the region of the flow that is disturbed by the model.

The measured incident mean wind speed profile resembles a power-law expression with exponent 0.15. The reference incident wind speed U_0 at 5 mm height (pedestrian-level; 2 m in full scale) was 5.9 m/s. The turbulence intensity of the incident flow, based on the local mean wind speed, ranged from 20% at 5 mm height to 5% at gradient height (0.9 m; 360 m full scale). The building models were rectangular and were placed parallel to each other, side-by-side (Figure 2). For all building configurations the blockage ratio was lower than 1%. Wind speed and turbulence intensity measurements were made with a TSI hot film anemometer along the passage centre line, at pedestrian height.

3.2. Numerical simulation and validation: initial results

Model validation is performed for the situation with two buildings of equal height and for wind direction parallel to the passage centre line, since these are the conditions studied in this paper. The building configuration is shown in Figure 2. The dotted line along the passage length, at a height of 2 m (full scale) above ground, is referred to as the passage centre line. Measurements are available at each dot: x = 0, 0.2D, 0.4D, 0.6D, 0.8D, 1D with D the building depth (= passage length).

In this subsection, the CFD simulation is performed according to common practice for near-ground ABL flow in commercial codes, i.e. by employing a high grid resolution near the bottom of the computational domain (small y_P) and by adhering to the requirement $K_S < y_P$. The 3D simulations are conducted at a scale of 1/40 (further referred to as "simulation scale") with the reference wind speed U_0 mentioned above. The reason for the different scale is to obtain suitable values for the non-dimensionless wall unit y^+ (between 30 and 100) for the use of wall functions, without the need to change the reference wind speed or the grid resolution for this purpose. Note that calculations at the reduced scale are allowed because to a first approximation, the location of the separation points at the building surface and the general flow features around the buildings can be considered to be independent of the Reynolds number. The dimensions of the computational domain are $L_D x W_D x H_D$ = 20.5x14x18 m³ (820x560x720 m³ in full scale). The building model is placed at a distance of 5 m (simulation scale, 200 m in full scale) from the inlet of the domain. The blockage ratio is 0.4%. A hybrid grid was constructed, the resolution of which was determined by some grid-sensitivity analyses based on refinements with a factor of 2. Figure 3a shows the grid at the bottom of the computational domain. Figure 3b is a perspective

view of the grid at the building surfaces and at the ground surface. The grid is a combination of a structured hexahedral grid, an unstructured wedge grid and an unstructured tetrahedral grid. A structured hexahedral grid is employed in the vicinity of the buildings (facades and roof) and in the passage (Fig. 3b) for higher accuracy. A structured grid is also used in the upstream, downstream and lateral regions relatively far away from the buildings (Fig. 3a). An unstructured grid with wedge cells is used to economically bridge the region between both hexahedral-cell regions horizontally (Fig. 3a-b). The unstructured grid with tetrahedral cells is used to vertically bridge the region between the fine hexahedral cells near the top of the building and the coarse hexahedral cells near the top centre of the domain. The use of the unstructured grids avoided the use of a large number of unnecessary cells in regions away from the building, which led to a significant reduction in the total number of cells. The total number of cells ranged between 0.9×10^6 and 10^6, dependent on the passage width. The distance y_P between the centre point of the wall-adjacent cells and the ground surface, which is important for the value of y^+, is 0.005 m (simulation scale) or 0.2 m (full scale). The value of y_P near the building model walls is about 0.0018 m (simulation scale) or 0.072 m (full scale).

The inlet mean wind speed profile and the turbulence intensity profile are taken equal to the measured incident wind tunnel profiles. The measured longitudinal turbulence intensity I_U is converted to turbulent kinetic energy k as input for the simulations using $k = 0.5(I_U U)^2$, assuming that $\sigma_v << \sigma_u$ and $\sigma_w << \sigma_u$.. Note that with a higher k, a small discrepancy in the results in the order of a few percentages (<5%) in the magnitude of amplification factors was found. The inlet turbulence dissipation rate profile is given by:

$$\varepsilon(y) = \frac{(u^*_{ABL})^3}{\kappa(y + y_0)} \tag{12}$$

where y is the height co-ordinate, κ the von Karman constant (~ 0.42), y_0 the scaled aerodynamic roughness length corresponding to a power-law exponent of 0.15 (here: $y_0 \approx 0.03$ m / 40 = 0.00075 m) and u^*_{ABL} the friction velocity related to a horizontally homogeneous (stable) ABL flow. Note that y_0 is obtained by fitting the log-law profile to the experimentally determined power-law profile. The sides and the top of the computational domain are modelled as slip walls (zero normal velocity and zero normal gradients of all variables). At the outlet, zero static pressure is specified.

The standard wall functions by Launder and Spalding (1974) modified for roughness as outlined in subsection 2.2 are employed. Note that the combination of the chosen simulation scale (1/40), the value for y_P and the reference wind speed U_0 taken from the wind tunnel experiments yields a suitable value of y^+ for the use of wall functions ($30 < y^+ < 100$). The values of K_S and C_{Ks} are needed as input. K_S for the bottom of the computational domain (representing the wind tunnel floor downstream of the roughness elements, including the turntable) is taken 2.5×10^{-6} m (simulation scale) or 0.0001 m (full scale), which is an estimate of the equivalent sand-grain roughness of the smooth floor. This value is smaller than y_P (= 0.005 m, simulation scale, 0.2 m in full scale) as required. Note that with $y_0 = 0.00075$ m, Eq. (1) is not satisfied. C_{KS} is set at its default value 0.5.

The commercial CFD code Fluent 6.1.22 is used to solve the 3D Reynolds-Averaged Navier-Stokes equations and the continuity equation using the control volume method. Closure is obtained using the realizable k-ε model (Shih et al. 1995). Pressure-velocity coupling is taken care of by the SIMPLE algorithm. Pressure interpolation is second order. Second order discretization schemes are used for both the convection terms and the viscous terms of the governing equations.

Figure 4 illustrates the initial calculation results together with the corresponding measurement data. The amplification factor is given along the passage centre line (K_{pcl}), at y = 2 m (full scale) and for a passage width w = 6 m (full scale). The measured amplification factor was obtained by division of the measured local wind speed U in the passage by the measured reference incident wind speed $U_0 = 5.9$ m/s. The CFD amplification factor was obtained by dividing the calculated local wind speed U by the same reference wind speed U_0. Figure 4 shows a general 15% discrepancy, although the measured and calculated profiles exhibit a similar shape. The reason for the shift of the curve is discussed in the next subsection.

3.3. Numerical simulation and validation: corrected results

The problem of horizontal inhomogeneity including the acceleration of the flow near the ground surface was discussed in subsection 2.3. The impact of horizontal inhomogeneity is assessed by performing a simulation in an empty 3D computational domain and by comparing the inlet profiles of wind speed and turbulence quantities with the simulated incident profiles. The simulation settings and characteristics are similar to those reported in the previous section, except for total number of grid cells because no buildings are present. The total number of

cells is only 190316. Figure 5 illustrates the simulation results in the empty domain in terms of the change of the vertical mean wind speed profile as it travels through the domain (*x = 0 m* is the inlet). Each profile represents the incident flow to which an obstacle at that position would be subjected. The observed acceleration of the wind speed profile corresponds to the statements made in subsection 2.3. It is clear that the predicted flow features will be largely influenced by these changes.

For the simulations with the building model, the upstream length was limited to 200 m (full scale). The difference between the inlet and incident profiles of mean wind speed and turbulence quantities is given in Figure 6. Note that U/U_0 is the amplification factor with U_0 = 5.9 m/s. While the difference between the inlet profiles (x = 0 m) and the incident flow profiles (x = 200 m) might seem to be insignificant at first sight (Fig. 6a), the differences in wind speed at the lowest 10 m are considerable (Fig. 6b). Even with an upstream length of only 200 m, the change in amplification factor at pedestrian level is 15%, causing the "CFD reference incident wind speed" to be 6.8 m/s instead of 5.9 m/s. It is important to note that in this case, due to the availability of turbulence intensity measurements, the inhomogeneity effect is still relatively limited. The frequently used expression for the inlet turbulent kinetic energy ($k = 3.3u^*_{ABL}{}^2$), in combination with the current roughness modifications, will generally give rise to even larger errors and larger increases in near-ground wind speed.

Neglecting the presence of horizontal inhomogeneity, the normal procedure would be to calculate the CFD amplification factors by division of the CFD wind speed U by U_0 = 5.9 m/s, yielding the results in Figure 4. To take the horizontal inhomogeneity into account, at least to some extent, the CFD reference wind speed is used: U_0 = 6.8 m/s. The difference in results and the comparison with the measurements are shown in Figure 7, which shows that a very close agreement with the measurements is indeed obtained with the corrected U_0.

4. Simulation results and analysis for different passage widths

The procedure for CFD simulations with corrections for horizontal inhomogeneity as outlined above has been used to perform additional CFD simulations for the same buildings but for a wide range of passage widths: w = 2, 4, 6, 8, 10, 15, 20, 30, 40, 60, 80, 100 m. The results of these simulations are briefly presented and analysed. The analysis is performed in terms of: (1) Pedestrian-level wind speed in the passages and in the corner streams; (2) Vertical wind-speed profiles in the passages; and (3) Flow rates (fluxes) through different planes in the passages.

4.1. Analysis of pedestrian-level wind speed

The maximum amplification factors at pedestrian-level height have been obtained along the passage centre line ($K_{pcl,max}$) and in the corner streams at the outer building corners ($K_{c,max}$), i.e. those that are not part of the passage. By analysis of a range of wind tunnel measurements, Stathopoulos et al. (1992) found that the ratio $K_{pcl,max}$ to $K_{c,max}$ seems to be an almost universal function of the ratio w/S, where w is the passage width and S is the building influence scale:

$$S = \left(B_L \, B_S^{\,2} \right)^{\frac{1}{3}} \tag{13}$$

The building influence scale was defined by Wilson (1989) for estimating dimensions of flow recirculation regions on building roofs. In Eq. (13), B_L is the larger and B_S is the smaller dimension of the windward facade. The CFD results from this study are superimposed on the data by Stathopoulos et al. (1992) in Figure 8. Note that the building dimensions in the simulations differ considerably from those in the particular experiments shown in Figure 8, but that nevertheless the CFD results show a very similar behaviour as the experimental results and there is quite a good agreement for the entire range of passage widths. The good results from these validation studies provide additional support for the analyses of the CFD results. Figure 9 shows contours of the amplification factor $K = U/U_0$ (where U is the magnitude of the 3D velocity vector) in a horizontal plane at pedestrian level for passage widths w = 2, 10, 30 and 100 m. The characteristics of the passage flow change significantly with varying passage width. Figure 10 repeats the universal relationship between $K_{pcl,max}/K_{c,max}$ and w/S. Based on Figures 9 and 10, three different regimes or types of passage flow at pedestrian level can be distinguished: (1) Resistance flow; (2) Interaction flow; and (3) Isolated flow. The ratio $K_{pcl,max}/K_{c,max}$ can be used to distinguish between these flow types because $K_{c,max}$ can be considered as a reference value: it is the value in the corner stream at the outer

building corner, and is equal to the maximum amplification factor in a passage with an infinitely large width. The regimes are indicated in Figure 10 and are discussed below.
1. *Resistance flow (w/S < 0.125).* For very narrow passages (e.g., w = 2 m, Fig. 9a), the ratio $K_{pcl,max}/K_{c,max}$ in the passage is close to one or even smaller than one, because of the high flow resistance in the passage. The maximum amplification factor anywhere in the passage, $K_{p,max}$, is situated at the passage centre line just beyond the passage entrance. No flow separation in the passage is observed.
2. *Interaction flow (0.125 ≤ w/S < 1.25).* For a wide range of passages (e.g., w = 10 m, Fig. 9b), the ratio $K_{pcl,max}/K_{c,max}$ is higher than one, indicating that the two corner streams originating and separating at the passage-entrance corners interact and merge together into a single wide passage jet, causing amplification factors higher than those in a single corner stream. $K_{p,max}$ is located somewhat further downstream compared with the resistance-flow type and the passage jet extends to a considerable distance downstream of the passage exit.
3. *Isolated flow (w/S ≥ 1.25).* The value *w/S = 1.25* marks the transition between interaction flow and isolated flow (w = 30 m, Fig. 9c). The ratio $K_{pcl,max}/K_{c,max}$ is equal to one indicating that there is no interaction of the corner streams in the passage anymore. For these passage widths, say w = 100 m (Fig. 9d), $K_{p,max}$ in the passage is no longer situated at the passage centre line but in the corner streams near the passage entrance corners. In these cases, two separate corner streams are clearly present in the passage.

Figure 11 illustrates the values of K_{pcl} at all positions along the passage centre line and for all passage widths in this study. Previous studies of pedestrian-level wind speed in passages between parallel buildings have been mainly concerned with passage widths ranging from 6 m to 12 m. For these values, the location of $K_{pcl,max}$ in the passage was found to vary to a lesser extent, which is confirmed by the results in Figure 11. Narrowing or widening the passage width beyond this range however, illustrates that both the value and the location of the maximum change significantly, as was also shown in Figure 9. For passage widths larger than 30 m, the maximum value is located at the exit of the passage.

Figure 12 provides the absolute values of the maximum amplification factors at different locations between and around the buildings as a function of the passage width. $K_{p,max}$ is the maximum found anywhere in the passage, i.e. either along the passage centre line or in the corner stream at the entrance of the passage. The maximum value of $K_{p,max} = K_{pcl,max}$ is found for a passage width w = 8 m and is about 1.47. Note that above w = 30 m, $K_{p,max}$ at the passage-entrance corner is almost identical to $K_{c,max}$ at the outer building corner and that both values are practically independent of the passage width. As a result, it can be stated that $K_{c,max}$ is nearly independent of the passage width.

4.2. Analysis of vertical wind speed profiles

Figure 13 shows amplification factors K_{pcp} along six vertical lines, located in the passage centre plane (pcp), for a passage width w = 6 m. The amplification factor K_{pcp} is defined as the ratio of the local wind speed at a certain position (x,y) to the wind speed at the same position without the buildings present, i.e. the "free-field" reference wind speed at the same height. As a result, K_{pcp} is a direct indication of the increase/decrease of the wind speed in the passage at all heights. The curves show a maximum near ground-level, due to the downflow of air at the windward facades that subsequently enters the passage near ground level. For this particular building configuration, the "vena contracta" in the passage causes a pronounced increase from x = 0 to x = 0.2D, at least in the lower part of the passage. In the upper part of the passage, the wind speed is actually decreased. The very pronounced increase of wind speed in the passage is thus limited to the near-ground level and is not an overall phenomenon in the passage. This observation is attributed to two reasons: (1) the pressure gradient over the passage length is more pronounced near ground level and (2) there is a considerable amount of air leaving the passage through the top plane, as will be shown in the next subsection.

4.3. Analysis of fluxes and the Venturi-effect

To evaluate the Venturi-effect an analysis of the overall flow through the passage is needed, rather than only the flow at pedestrian-level or in the passage centre plane. Figure 14 shows the three fluxes defined for this purpose: the flux of air F_P through the vertical plane A_P at the passage entrance, the flux F_V through the horizontal plane A_v at the top of the passage and the flux F_F through a vertical plane A_F that is identical to plane A_P but without the buildings present ("free" flux). Since building depth and height are equal in this study, the areas of the planes A_P and A_V are the same. The presence of the Venturi-effect should imply a significant increase in flow rate F_P through the passage compared to the "free" flow rate F_F. Figure 15a however shows that the flow rate through the passage is only increased by a very small amount (at most 8%) in spite of the

significant flow contraction. For larger passage widths, it is even lower than the free-field flux. The ratio F_P/F_F shows no clear proportionality to the decrease of the flow section. The reason is the wind-blocking effect by the buildings in combination with the flow resistance in the passage for the narrower passage widths. The wind-blocking effect implies that the flow will rather go over and around the buildings instead of being forced through the passage, as discussed and illustrated by Blocken et al. (2005) and Blocken and Carmeliet (2006). Based on these results, a better term to describe the flow conditions in passages might be the "channeling effect", which applies to the wind direction rather than to the amplification of wind speed. In addition, Figure 15b shows that especially for the narrower passages the flow resistance in the passage yields a considerable vertical flux out of the passage. For the narrowest passage, the vertical flux F_V is 40% of the passage flux. For wider passages, the ratio F_V/F_P rapidly decreases. This vertical flux is partly responsible for the decrease of the wind speed values in the passage as they travel along the x-axis, as illustrated in Figure 13. This decrease will be more pronounced as the passage width becomes narrower.

5. Discussion

With the type of roughness modification outlined in this paper, satisfying all four requirements mentioned in section 2 for CFD simulations of near-ground ABL flows is generally impossible. The results show that the resulting horizontal inhomogeneity of the vertical flow profiles in the upstream part of the computational domain can seriously compromise the accuracy of CFD simulations. When horizontal inhomogeneity is pronounced, no acceptable correspondence between CFD simulations and measurements can be expected, no matter how accurate both of them were conducted. Therefore, remedial measures are imperative.

Apart from the rather simple correction that was applied in this paper, various other remedial measures can be suggested to reduce the consequences of horizontal inhomogeneity. In CFD simulations with commercial CFD codes, different remedial measures – although not always mentioned explicitly – were applied by e.g. Miles and Westbury (2003), Blocken et al. (2004, 2005), Blocken and Carmeliet (2004, 2006), Franke and Frank (2005) and Moonen et al. (2006). However, none of these approaches has shown an overall acceptable performance in all situations. Research work on other remedial measures is currently ongoing. To the authors' opinion, the best solution to the wall-function-roughness problem is to satisfy all four requirements for CFD simulation of ABL flow by implementing wall functions with roughness modifications that are specifically derived for and adapted to both the inlet profiles and the turbulence model used in the simulation. These functions should be derived by taking into account the requirement of horizontal homogeneity, without the need for large near-ground cells, and should be applied in the upstream and downstream regions of the domain away from the building model(s). For the standard k-ε turbulence model, an appropriate set of inlet profiles and wall functions was provided by Richards and Hoxey (1993) in terms of an analytical solution of the standard k-ε model to determine the model constant σ_ε. However, most commercial CFD codes currently do not allow implementation of other wall functions. In general, for every CFD simulation, it is advised to at least assess the effects of horizontal inhomogeneity by first performing a simulation in an empty computational domain.

Strictly speaking the requirement for horizontal homogeneity does not apply when the intent of the CFD simulation is the development of an internal boundary layer starting from the inlet of the computational domain. In this case however, similar problems will often be present, thus simulations in an empty domain are advised to validate the CFD simulation of the IBL before conducting the simulations with the building models present.

6. Summary and conclusions

The study described in this paper has found the following:

- The "modified-for-roughness" wall functions currently implemented in many commercial CFD codes are based on experimental data for flow over sand-grain roughened surfaces. These functions may be useful for modelling flow in roughened pipes and channels but can be unsuitable for the simulation of flow in the atmospheric boundary layer (ABL). Their use can give rise to horizontal inhomogeneity of the mean wind speed and turbulence profiles. Simulating a horizontally homogeneous ABL flow is essential for accurate CFD simulations in building-related studies. Horizontal inhomogeneity can at least partly be held responsible for the large discrepancies that are sometimes found between numerical results and the corresponding measurement data in building-structure interaction studies, pedestrian-level wind studies, studies of pollutant dispersion, wind-driven rain, etc.

- In general, for every CFD simulation, it is advised to assess the effects of horizontal inhomogeneity by first performing a simulation in an empty computational domain before conducting simulations with the building models present.
- Three different regimes of flow conditions in passages between buildings can be distinguished: resistance flow, interaction flow and isolated flow. The wind tunnel studies by Stathopoulos et al. (1992) and the numerical study in this paper indicate that these regimes appear to occur within a well-defined, almost universal range of the ratio w/S, i.e. the passage width divided by the building influence scale.
- At least for the cases studied here, there is no general increase of wind speed in the passage over the total height of the passage. The well-studied and significant increase in pedestrian-level wind speed in passages between buildings is present, but it is limited to ground-level. At higher levels in the passage, the wind speed actually decreases compared to free-field conditions. This is accompanied by a significant amount of air leaving the passage through the top horizontal plane of the passage volume.
- For the building configurations and incident flow conditions studied here, the flow rate through a vertical plane in the passages is at most only slightly higher than the flow rate through a similar vertical plane in free-field conditions (no buildings present). This implies that the Venturi-effect is rather weak in such configurations. A better term to describe the flow conditions in passages might be the "channeling effect", which applies to the wind direction rather than to the amplification of wind speed.
- This study concerning the wind speed conditions in passages was limited to buildings with fixed and identical dimensions and was conducted with given incident flow profiles. As a result, further research is needed to expand the validity of the present findings, especially concerning the Venturi-effect.

Acknowledgements

The first author has been a post-doctoral research fellow of the FWO-Flanders (Research Fund – Flanders), an organization that supports and stimulates fundamental research in Flanders (Belgium). This research has been conducted while the first author was at the Centre for Building Studies, Department of Building, Civil and Environmental Engineering, Concordia University, Montreal and while he was also supported by the FWO-Flanders. The authors want to express their gratitude for this significant financial support. We also thank Ir. David Dooms for his kind help during the completion of this paper and the anonymous reviewers for their clear and valuable comments.

Nomenclature

A	exponential roughness function (dimensionless)
A_F	area of the vertical plane in free-field conditions (m²)
A_P	area of the vertical plane in the passage (m²)
A_V	area of the horizontal plane at the top of the passage (m²)
B_L, B_S	larger and smaller dimension of the windward facade (m)
C_{Ks}	roughness constant (dimensionless)
C_μ	constant in the standard k-ε model, variable in the realizable k-ε model (dimensionless)
D, L, H	building depth, length, height (m)
F	flux through planes in the passage (m³/s)
k	turbulent kinetic energy (m²/s²)
K_c	amplification factor in corner stream at outer building corner (dimensionless)
K_{pcl}	amplification factor along passage centre line (dimensionless)
K_{pcp}	amplification factor in passage centre plane (dimensionless)
K_{max}	maximum amplification factor (dimensionless)
K_S	physical or geometrical roughness height (m)
L_D, W_D, H_D	length (streamwise), width (lateral) and height of computational domain (m)
P	centre point of the wall-adjacent cell
S	building influence scale (m)
u_{ABL}*	friction velocity associated with atmospheric boundary layer flow (m/s)
u*, u^+	wall-function friction velocities (m/s)
U	local wind speed (magnitude of the 3D velocity vector) (m/s)
U_0	reference incident wind speed at 2 m (full scale) (m/s)
U_P	tangential wind speed in the centre point P of the wall-adjacent cell (m/s)

w	passage width (m)
x, y, z	Cartesian co-ordinates (x: streamwise, y: height, z: lateral) (m)
y_0	aerodynamic roughness length (m)
y_P	distance from the centre of the wall-adjacent cell to the wall (m)
y^+	non-dimensionless wall unit
ε	turbulence dissipation rate (m^2/s^3)
ε_P	turbulence dissipation rate in the wall-adjacent cell (m^2/s^3)
κ	von Karman constant (~0.42) (dimensionless)
ν	kinematic viscosity (m^2/s)
ρ	fluid density (kg/m^3)
σ_u, σ_v, σ_w	standard deviation of turbulent fluctuations in x, y and z direction (m/s)
τ_w	wall shear stress (Pa)
ΔB	roughness function (dimensionless)

References

Ansys Ltd., 2005. Ansys CFX-solver, Release 10.0: Theory. Canonsburg.

Baskaran, A., Kashef, A., 1996. Investigation of air flow around buildings using computational fluid dynamics techniques. Engineering Structures 18, 11, 861-875.

Blocken, B., Carmeliet, J., 2004. A review of wind-driven rain research in building science. Journal of Wind Engineering and Industrial Aerodynamics 92, 13, 1079-1130.

Blocken, B., Roels, S., Carmeliet, J., 2004. Modification of pedestrian wind comfort in the Silvertop Tower passages by an automatic control system. Journal of Wind Engineering and Industrial Aerodynamics 92, 10, 849-873.

Blocken, B., Carmeliet, J., 2006. The influence of the wind-blocking effect by a building on its wind-driven rain exposure, Journal of Wind Engineering and Industrial Aerodynamics 94, 2, 101-127.

Blocken, B., Carmeliet, J., Stathopoulos, T., 2005. A numerical study on the existence of the Venturi-effect in passages between perpendicular buildings. in: Proceedings of the 6th Asia Pacific Conference on Wind Engineering (6APCWE), September 12-14 2005, Seoul, Korea, pp. 2633-2647.

Bottema, M., 1993. Wind climate and urban geometry, PhD thesis. FAGO. Technical University of Eindhoven.

Cebeci, T., Bradshaw, P., 1977. Momentum transfer in boundary layers. Hemisphere Publishing Corporation, New York.

Chang, C.H., Meroney, R.N., 2001. Numerical and physical modelling of bluff body flow and dispersion in urban street canyons. Journal of Wind Engineering and Industrial Aerodynamics 89, 14-15, 1325-1334.

Durbin, P.A., Petterson Reif, B.A., 2001. Statistical theory and modelling for turbulent flows, John Wiley & Sons, Chichester.

Fluent Inc., 2003. Fluent 6.1 User's Guide, Fluent Inc., Lebanon.

Franke, J., Hirsch, C., Jensen, A.G., Krüs, H.W., Schatzmann, M., Westbury, P.S., Miles, S.D., Wisse, J.A., Wright, N.G., 2004. Recommendations on the use of CFD in wind engineering, in: proceedings of the International Conference on Urban Wind Engineering and Building Aerodynamics, (Ed. van Beeck JPAJ), COST Action C14, Impact of Wind and Storm on City Life Built Environment, von Karman Institute, Sint-Genesius-Rode, Belgium, 5 - 7 May 2004.

Franke, J., Frank, W., 2005. Numerical simulation of the flow across an asymmetric street intersection, in: Proceedings of the 4th European and African Conference on Wind Engineering (4EACWE), 11-15 July 2005, Prague, Czech Republic.

Ishizaki, H., Sung, I.W., 1971. Influence of adjacent buildings to wind, in: Proceedings of the 3rd International Conference Wind Effects on Buildings and Structures, Tokyo, Japan, pp. I.15.1-I.15.8.

Kim, S.E., Choudhury, D., 1995. A near-wall treatment using wall functions sensitized to pressure gradient, Fluids Engineering Division – ASME 217, Separated and Complex Flows, 1995.

Launder, B.E., Spalding, D.B., 1974. The numerical computation of turbulent flows, Computer Methods in Applied Mechanics and Engineering 3, pp. 269-289.

Leitl, B., 2000. Validation Data for Microscale Dospersion Modelling, EUROTRAC newsletter 22/2000.

Leitl, B., Schatzmann, M., 1999. Generation of High Resolution Reference Data for Validation of Microscale Dispersion Models, in: VDI-Berichte 1443, Recent Developments in Measurement and Assessment of Air Pollution, VDI-KRdL 1999, pp. 647-656.

Ligrani, P.M., Moffat, R.J., 1986. Structure of transitionally rough and fully rough turbulent boundary layers. Journal of Fluid Mechanics 162, 69-98.
Mathews, E.H., 1987. Prediction of the wind-generated pressure distribution around buildings. Journal of Wind Engineering and Industrial Aerodynamics 25, 219-228.
Miles, S., Westbury, P., 2003. Practical tools for wind engineering in the built environment. QNET-CFD Network Newsletter, 2, 2, 11-14.
Moonen, P., Blocken, B., Roels, S., Carmeliet, J., 2006. Numerical modeling of the flow conditions in a low-speed closed-circuit wind tunnel. Journal of Wind Engineering and Industrial Aerodynamics. In press. (doi:10.1016/j.jweia.2006.02.001).
Richards, P.J., Hoxey, R.P., 1993. Appropriate boundary conditions for computational wind engineering models using the k-ε turbulence model. Journal of Wind Engineering and Industrial Aerodynamics 46&47, 145-153.
Richards, P.J., Younis, B.A., 1990. Comments on "Prediction of the wind-generated pressure distribution around buildings" by Mathews EH, Journal of Wind Engineering and Industrial Aerodynamics 34,107-110.
Shih, T.H., Liou, W.W., Shabbir, A., Zhu, J., 1995. A new k-ε eddy-viscosity model for high Reynolds number turbulent flows – model development and validation. Computers and Fluids 24, 3, 227-238.
Stathopoulos, T., Storms, R., 1986. Wind environmental conditions in passages between buildings. Journal of Wind Engineering and Industrial Aerodynamics 24, 19-31.
Stathopoulos, T., 1984. Design and fabrication of a wind tunnel for building aerodynamics. Journal of Wind Engineering and Industrial Aerodynamics 16, 361-376.
Stathopoulos, T., Wu, H., 1995. Generic models for pedestrian-level winds in built-up regions. Journal of Wind Engineering and Industrial Aerodynamics 54-55, 515-525.
Stathopoulos, T., Wu, H., Bédard, C., 1992. Wind environment around buildings: a knowledge-based approach. Journal of Wind Engineering and Industrial Aerodynamics 41-44, 2377-2388.
To, A.P., Lam, K.M., 1995. Evaluation of pedestrian-level wind environment around a row of tall buildings using a quartile-level wind speed descripter. Journal of Wind Engineering and Industrial Aerodynamics 54-55, 527-541.
Wieringa, J, 1992. Updating the Davenport roughness classification, Journal of Wind Engineering and Industrial Aerodynamics 41-44, 357-368.
Wilson, D.J., 1989. Airflow around buildings, ASHRAE Handbook of Fundamentals, pp. 14.1-14.18.
Wiren, B.G., 1975. A wind tunnel study of wind velocities in passages between and through buildings, in: Proceedings of the 4th Int. Conf. Wind Effects on Buildings and Structures, Heathrow 1975, Cambridge University Press, pp. 465-475.

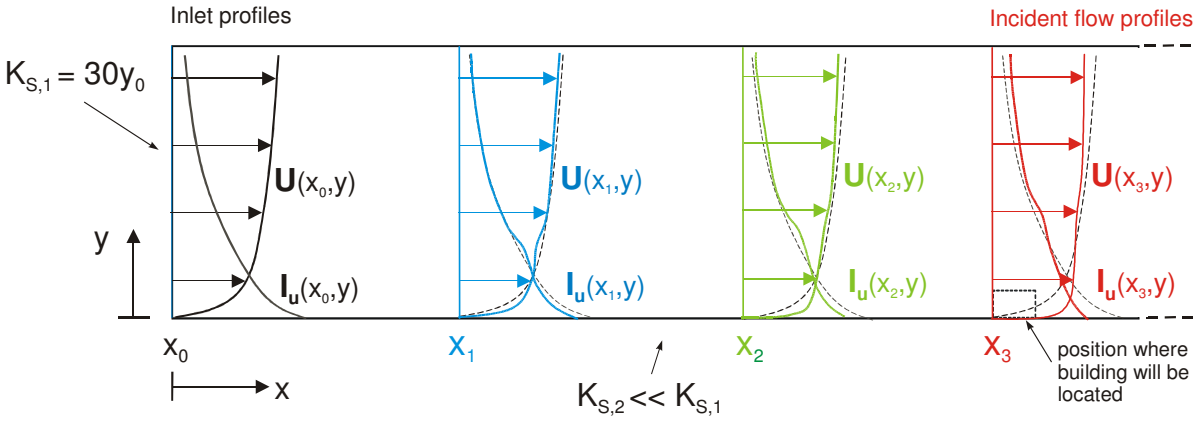

Figure 1. Schematic illustration of the development of an internal boundary layer (horizontal inhomogeneity) in a CFD simulation in an empty domain with ground roughness $K_{S,2}$ instead of $K_{S,1}$.

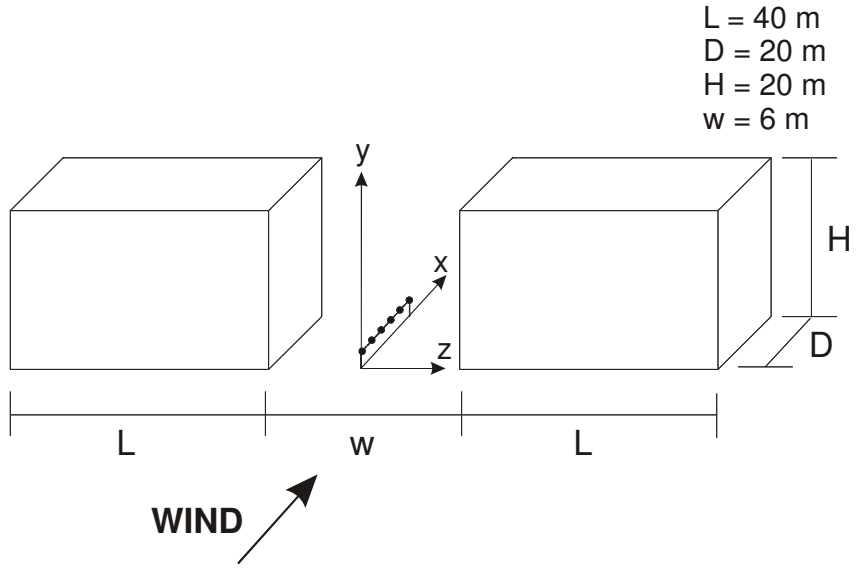

Figure 2. Building configuration used for model validation with indication of the passage centre line.

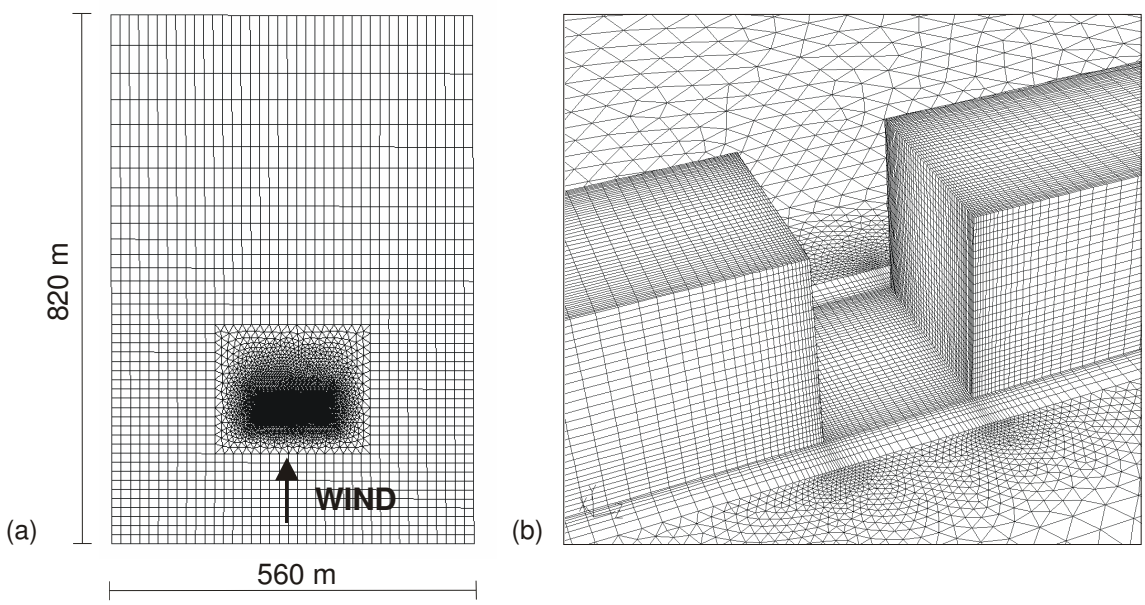

Figure 3. (a) Top view of the grid at the bottom of the 3D computational domain. (b) Perspective view of the grid near the buildings and in the passage.

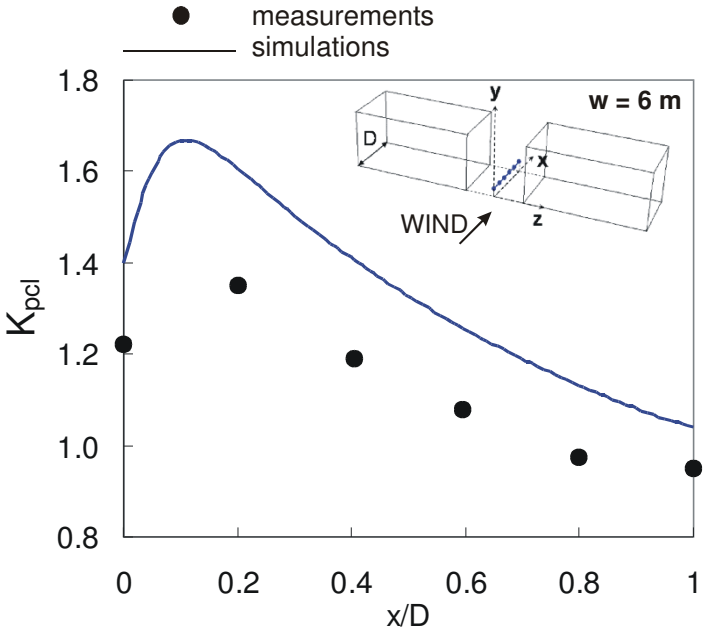

Figure 4. Measured and calculated amplification factors K_{pcl} along the passage centre line for the initial simulation.

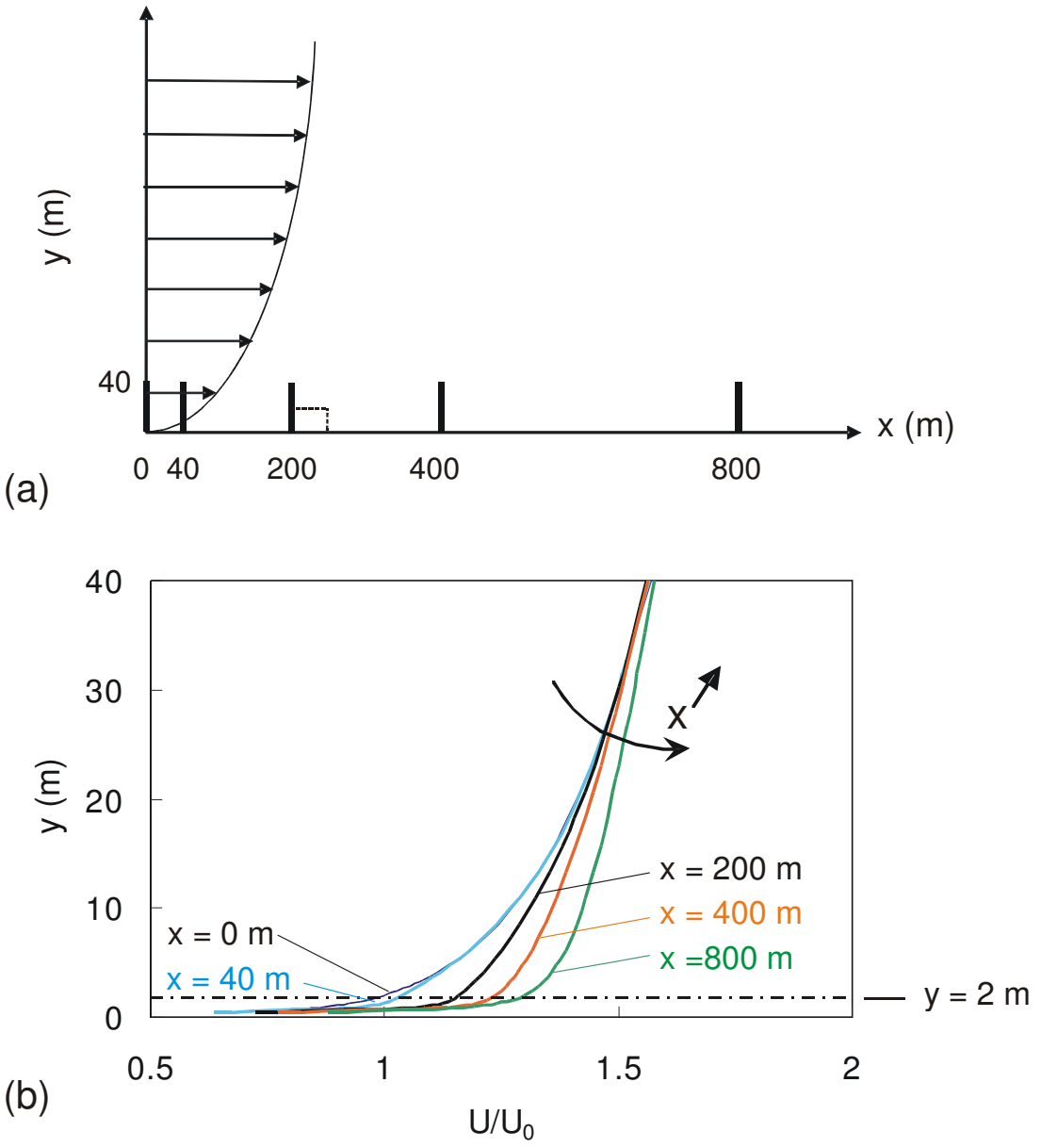

Figure 5. (a) Positions of vertical lines in part of an empty computational domain identical to the domain with building models. The position where the building would be situated is indicated (dashed lines at x = 200 m). (b) Calculated profiles of mean wind speed along the vertical lines to illustrate the acceleration near the ground surface (horizontal inhomogeneity).

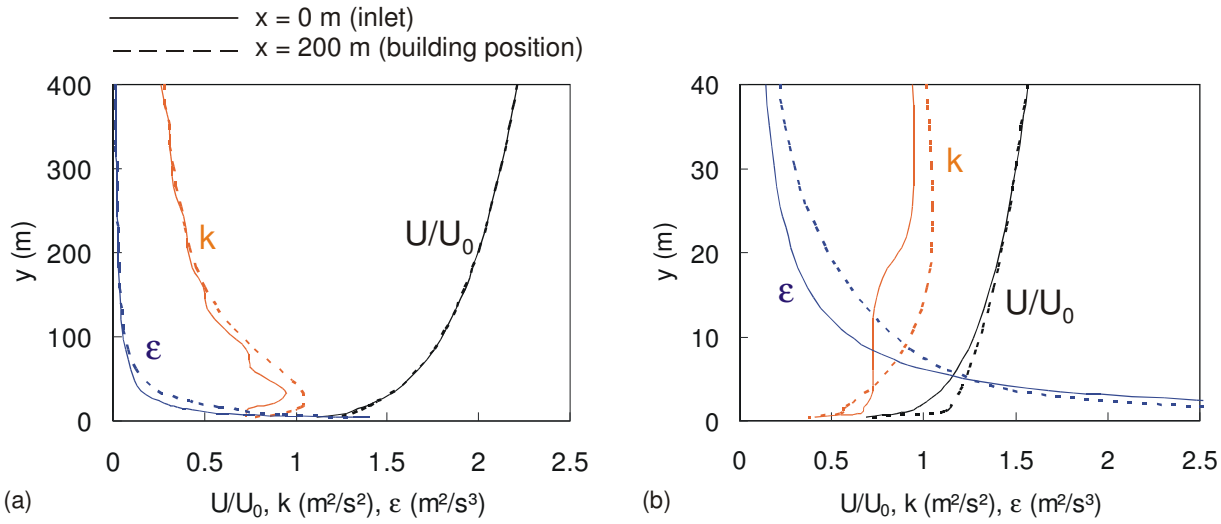

Figure 6. Vertical profiles of amplification factor U/U_0, turbulent kinetic energy k and turbulence dissipation rate ε in an empty computational domain, at the inlet of the computational domain (approach flow) and where the buildings would be positioned (incident flow). (a) From 0 m to 400 m, (b) From 0 m to 40 m (= twice the building height).

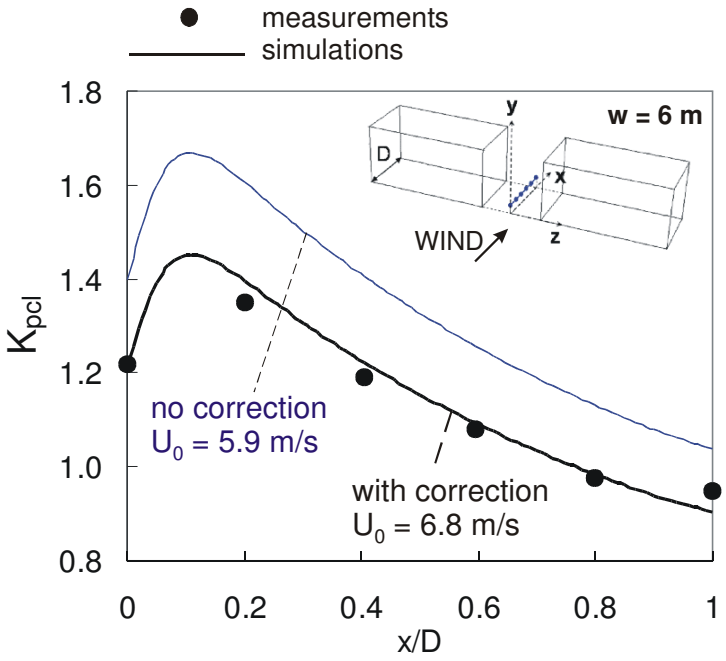

Figure 7. Measured and calculated amplification factors K_{pcl} along the passage centre line before and after correction for horizontal inhomogeneity.

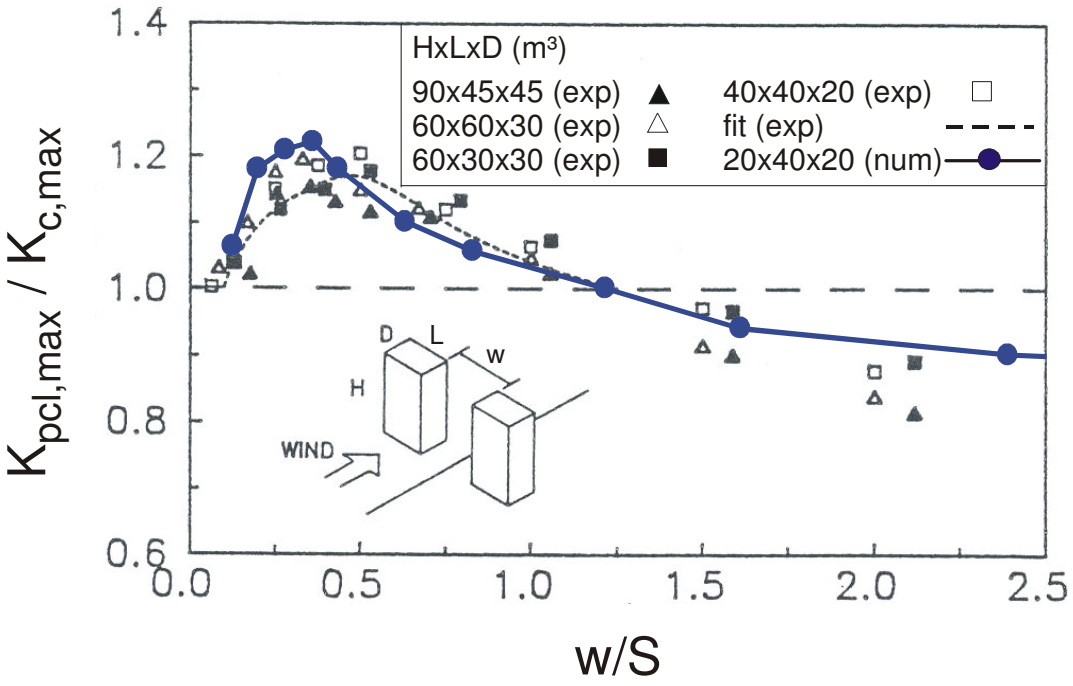

Figure 8. Ratio of the maximum amplification factor along the passage centre line $K_{pcl,max}$ and in the corner stream $K_{c,max}$ as a function of the ratio between passage width w and building influence scale S.

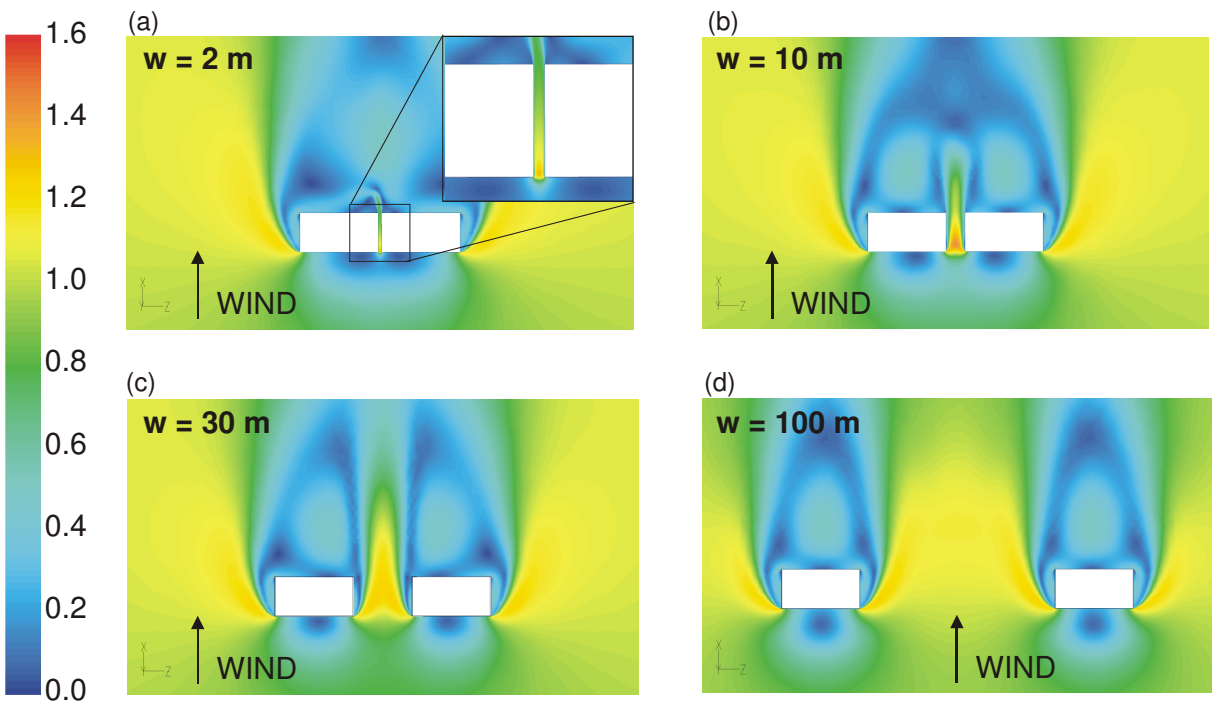

Figure 9. Contours of amplification factor K in a horizontal plane at pedestrian level (y = 2 m) for four passage widths.

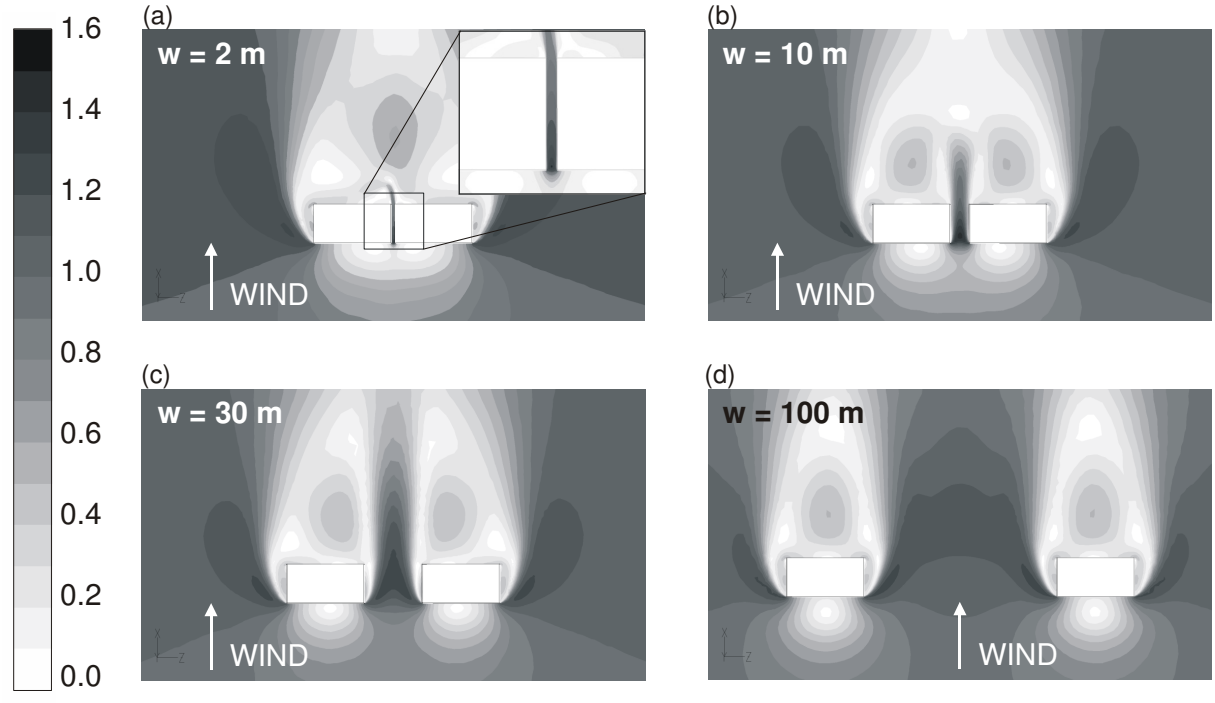

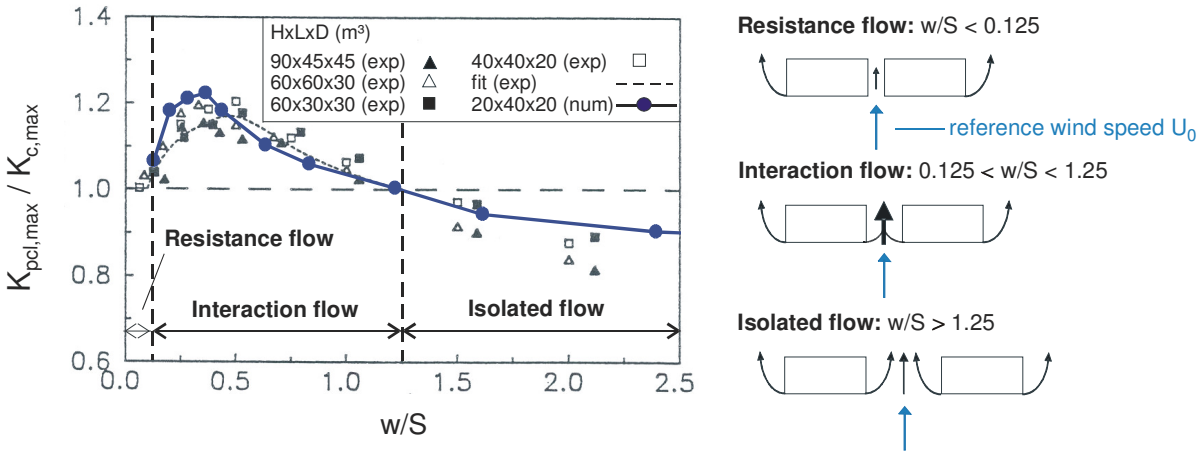

Figure 10. Definition and schematic representation (right, top views) of the three flow regimes for pedestrian-level wind speed in passages.

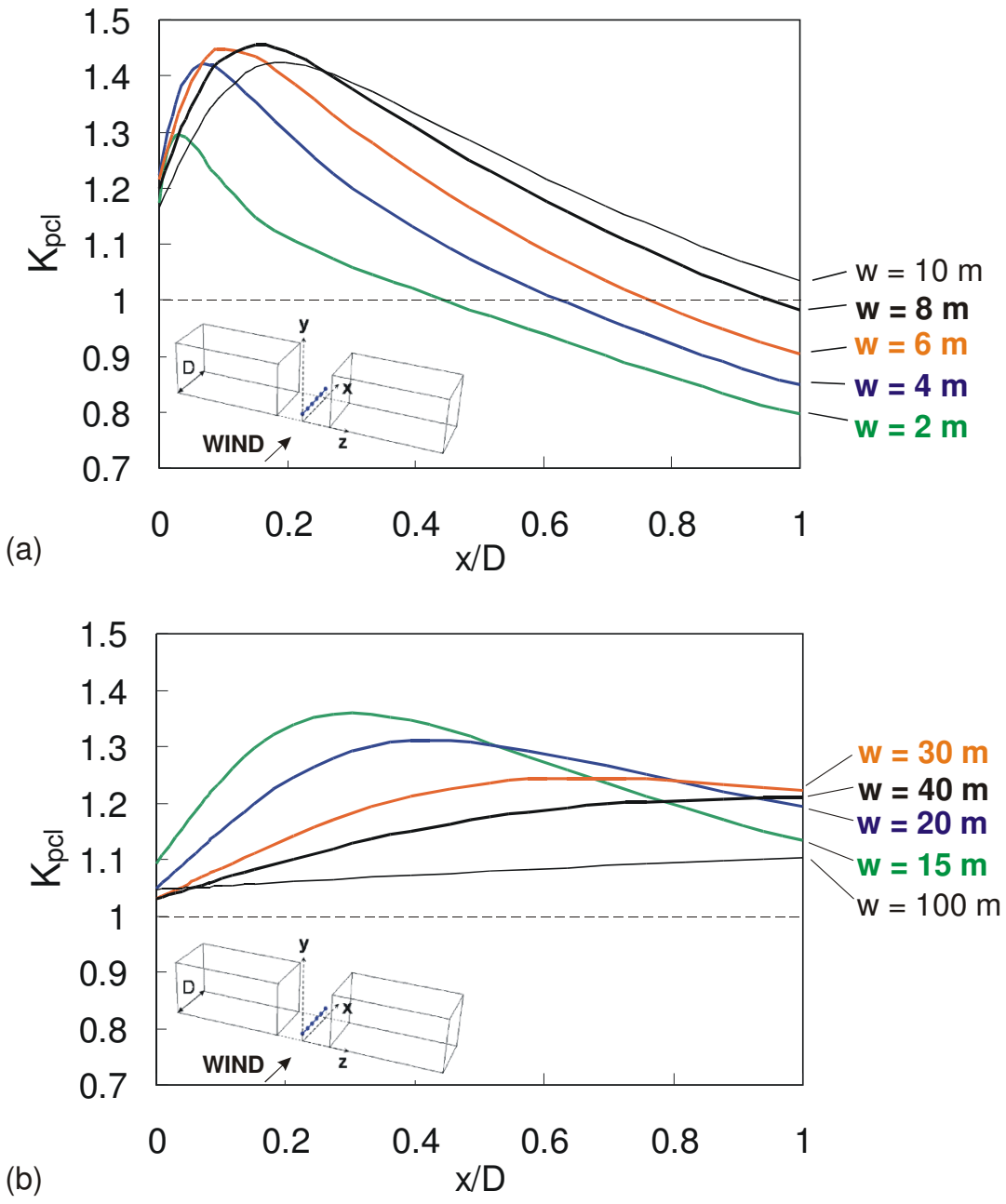

Figure 11. Amplification factor K_{pcl} along the passage centre line (y = 2 m, pedestrian height) for different passage widths.

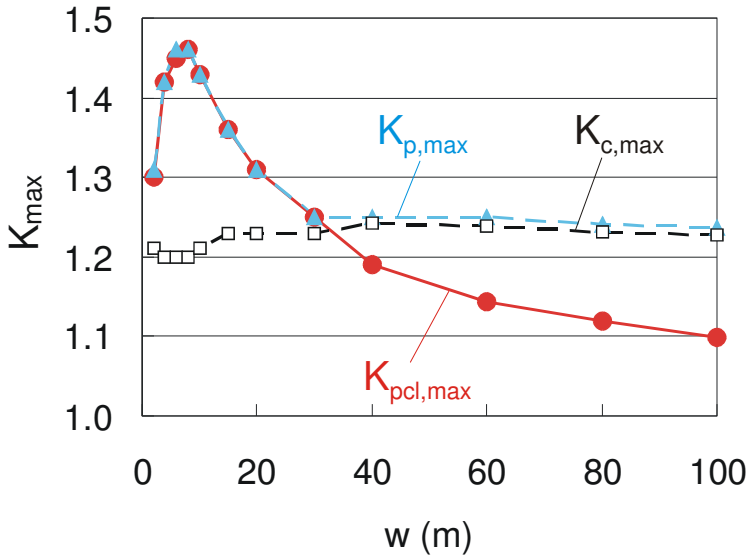

Figure 12. Maximum amplification factors $K_{pcl,max}$ (along passage centre line), $K_{p,max}$ (anywhere in the passage) and $K_{c,max}$ (in the corner stream at the outer building corner), all at y = 2 m (pedestrian height), as a function of the passage width.

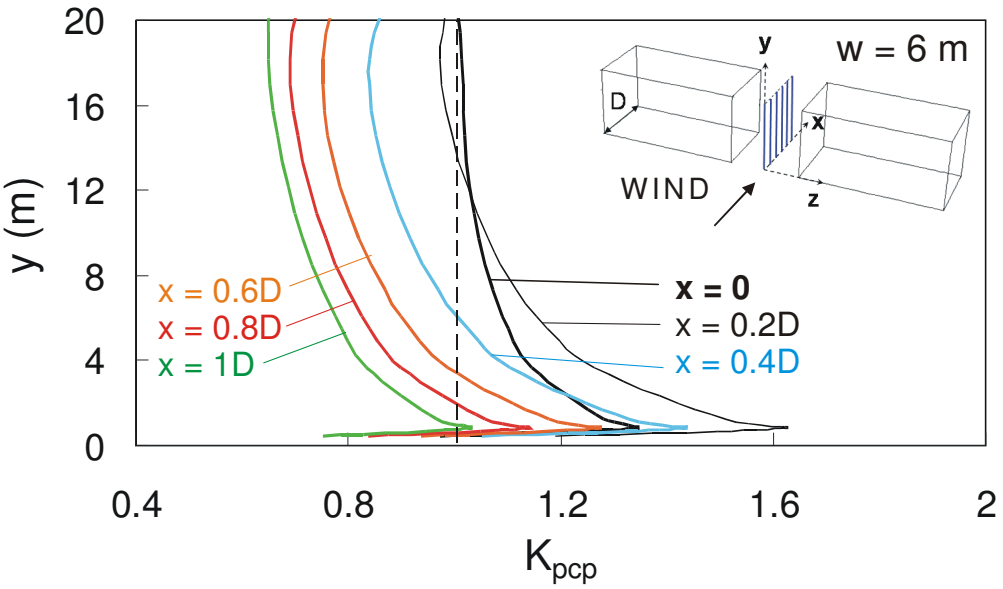

Figure 13. Vertical profiles of the amplification factor K_{pcp} in the passage centre plane (pcp) along six vertical lines at equidistant positions: x = 0, 0.2D, 0.4D, 0.6D, 0.8D, 1D.

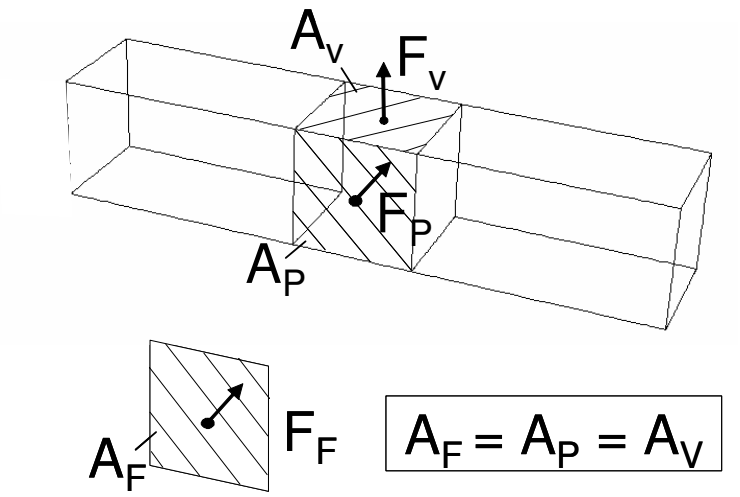

Figure 14. Illustration and notations of passage areas and passage fluxes.

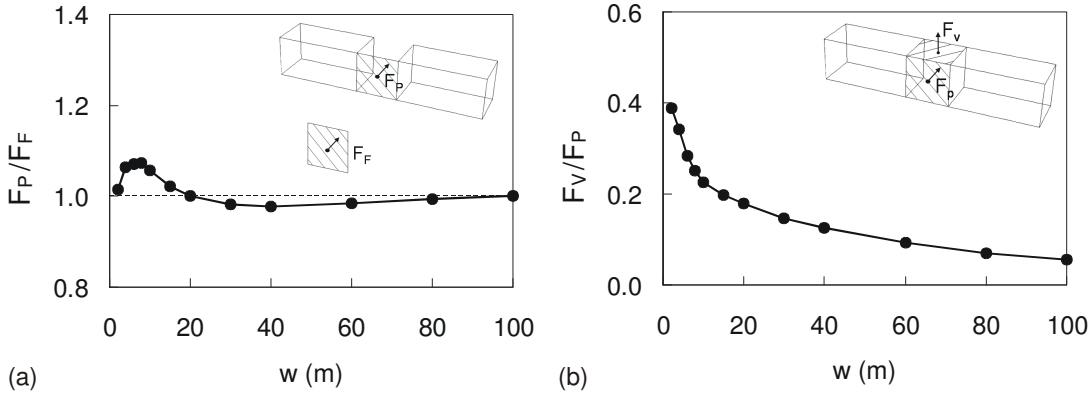

Figure 15. (a) Ratio of passage flux F_P to free-field flux F_F. (b) Ratio of vertical passage flux F_V to passage flux F_P.